

# Induced-charge electro-osmosis

By **TODD M. SQUIRES<sup>1</sup> AND MARTIN Z. BAZANT<sup>2</sup>**

<sup>1</sup>Departments of Applied and Computational Mathematics and Physics,  
California Institute of Technology, Pasadena, CA 91125

<sup>2</sup>Department of Mathematics and Institute for Soldier Nanotechnologies,  
Massachusetts Institute of Technology, Cambridge, MA 02139

(Received 28 October 2019)

The general phenomenon of ‘induced-charge electro-osmosis’ (ICEO) is described — the nonlinear electro-osmotic slip caused by an applied field acting on induced ionic charge in the vicinity of a polarizable surface. A simple physical picture of the basic phenomenon is presented, and the ICEO flow around conducting cylinders and spheres in steady (DC), oscillatory (AC), and suddenly-applied electric fields is calculated, providing perhaps the simplest and clearest example of a non-equilibrium electrokinetic phenomenon. It is shown that ICEO slip velocities generally vary like  $u_s \propto E_0^2 a$  in uniform fields, where  $E_0$  is the applied field strength and  $a$  is a geometrical length scale, and are set up on a time scale  $\tau_c = \lambda_D a / D$ , where  $\lambda_D$  is the screening length and  $D$  the diffusion constant of the electrolytic ions. A variety of microfluidic flows results for conducting objects of either fixed total charge or fixed potential. The effect of a dielectric coating upon ICEO flows is also calculated and illustrates two points: (i) ICEO occurs around polarizable dielectric surfaces, in addition to conducting surfaces, and (ii) a thin dielectric layer reduces the ICEO slip velocity, particularly when the coating is thicker than the screening length. Finally, the effective equations are re-derived from the basic equations of ionic transport and fluid flow by matched asymptotic expansions in the thin double-layer limit, thus firmly justifying their use here and in more general situations of ICEO. Fundamental implications of ICEO for colloidal science and microfluidics are also discussed.

---

## 1. Introduction

Recent developments in micro-fabrication and the continuing importance of electro-phoretic techniques in analytical chemistry and molecular biology has brought a renewed interest to the study of electrokinetics. New challenges have arisen with the advent of microfluidic devices: On micron length scales, the familiar techniques used in larger-scale applications for fluid manipulation do not work due to the enhancement of viscous damping. Furthermore, due to the low Reynolds numbers of microfluidic devices, the mixing of miscible fluids must occur without the benefit of turbulence, by molecular diffusion alone. A variety of innovative ideas are thus being considered for pumping, mixing, manipulating and separating on the micron length scale, naturally focusing on the use of surface phenomena.

### 1.1. Standard (‘fixed-charge’) electro-osmosis

Electrokinetic techniques provide some of the most popular small-scale non-mechanical strategies for manipulating particles and fluids. We present here a very brief introduction; for a more detailed account, the reader is referred to, *e.g.*, Russel *et al.*(1989). A surface with charge density  $q_0$  in an aqueous solutions attracts a screening cloud of

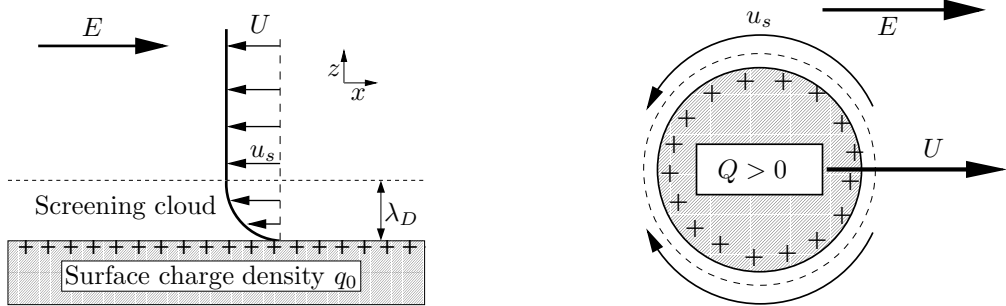


FIGURE 1. Left: A charged solid surface in an electrolytic solution attracts an oppositely-charged ‘screening cloud’ of width  $\sim \lambda_D$ . An electric field applied tangent to the charged solid surface gives rise to an electro-osmotic flow, with magnitude given by Eq. (1.4). Right: An electric field applied to an electrolytic solution containing a suspended solid particle gives rise to particle motion called electrophoresis, with velocity equal in magnitude and opposite in direction to Eq. (1.4).

oppositely-charged counter-ions to form the electrochemical ‘double layer’, effectively a surface capacitor. The excess diffuse ionic charge exponentially screens the electric field set up by the surface charge (Fig. 1a), giving an electrostatic potential

$$\phi = \frac{q_0}{\epsilon_w \kappa} e^{-\kappa z} \equiv \zeta e^{-\kappa z}. \quad (1.1)$$

Here  $\epsilon_w \approx 80\epsilon_0$  is the dielectric constant of water (and  $\epsilon_0$  is the vacuum permittivity), the ‘zeta potential’, defined by

$$\zeta \equiv \frac{q_0}{\epsilon_w \kappa}, \quad (1.2)$$

reflects the electrostatic potential drop across the screening cloud, and the Debye ‘screening length’  $\kappa^{-1}$  is defined for a symmetric 1:1 electrolyte by

$$\kappa^{-1} \equiv \lambda_D = \left( \frac{2n_0 e^2}{\epsilon_w k_B T} \right)^{1/2}, \quad (1.3)$$

with bulk ion concentration  $n_0$ , (monovalent) ion charge  $e$ , Boltzmann constant  $k_B$  and temperature  $T$ . For simplicity, we assume zeta potentials to be small ( $\zeta \ll k_B T/e$ ), so that the Poisson-Boltzmann equation for electrolyte screening can be linearized, giving the linear relationship in equation (1.2). The more general case of nonlinear screening is conceptually the same as the linearized case, but requires a nonlinear relationship  $\zeta(q_0)$  in place of equation 1.2.

An externally applied electric field exerts a body force on the electrically charged fluid in this screening cloud, driving the ions and the fluid into motion. The resulting *electro-osmotic* fluid flow (Fig. 1a) appears to ‘slip’ just outside the screening layer of width  $\lambda_D$  with local slip velocity given by the classical Helmholtz-Smoluchowski formula,

$$\mathbf{u}_s = -\frac{\epsilon_w \zeta}{\eta} \mathbf{E}_{||}, \quad (1.4)$$

where  $\eta$  is the fluid viscosity and  $\mathbf{E}_{||}$  is the tangential component of the bulk electric field. Remarkably, equation (1.4) holds for arbitrary zeta potentials, even in the regime of nonlinear screening, as long as the double layer is thin compared to the radius of curvature of the surface.

This basic electrokinetic phenomenon gives rise to two related effects, electro-osmosis

and electrophoresis, both of which find wide application in analytical chemistry, microfluidics, colloidal self-assembly, and other emerging technologies. Electro-osmotic flow occurs when an electric field is applied along a channel with charged walls, wherein the electro-osmotic slip at the channel walls gives rise to plug flow in the channel, with velocity given by equation (1.4). Because the electro-osmotic flow velocity is independent of channel size, (in contrast to pressure-driven flow, which depends strongly upon channel size), electro-osmotic pumping presents a natural and popular technique for fluid manipulation in small channels.

On the other hand, when the solid/fluid interface is that of a freely-suspended particle, the electro-osmotic slip velocity gives rise to motion of the particle itself (Figure 1b), termed *electrophoresis*. In the thin double-layer limit, the electrophoretic velocity is

$$U = \frac{\epsilon_w \zeta}{\eta} E_\infty \equiv \mu_e E_0, \quad (1.5)$$

where  $E_0$  is the externally-applied field, and  $\mu_e = \epsilon_w \zeta / \eta$  is the electrophoretic mobility of the particle. Morrison(1970) derived several rather astonishing results in the thin double-layer limit: 1) The electrophoretic mobility  $\mu_e$  is independent of particle size, shape, or number; 2) multiple particles of the same zeta potential (but possibly different shape and size) experience identically zero interaction; and 3) the fluid flow is a potential flow, everywhere directed along electric field lines. His conclusions were based upon the observation that, when all surfaces have the same zeta potential, a proposed velocity potential obeys the same equation and boundary conditions as the electrostatic potential.

The central assumption in Morrison's work, and in almost all subsequent work, is that of a constant zeta potential on the particle surface. Ajdari(1996) has pointed out some interesting consequences when this assumption is violated by deliberately patterning surfaces in an inhomogeneously-charged fashion. For example, electrophoresis can occur in a different directions, even *opposite* to that expected from the particle's mean zeta potential.

A conducting or (surface-reactive) particle whose equilibrium surface charge density is homogeneous would attain an inhomogeneous surface charge in non-equilibrium situations. This might be expected to affect the electrophoretic mobility of such a particle. Remarkably, however, this does not occur. In considering the electrophoretic motion of a metal colloid, Levich(1962) discussed the non-uniform surface charge that results when free charges rearrange themselves in order to maintain an equipotential surface, but pursued it only far enough to demonstrate that the electrophoretic mobility depends only on the equilibrium zeta-potential. O'Brien & White(1978) followed this with a more general proof — valid for arbitrary diffuse layer thickness, particle composition and chemistry — that the electrophoretic mobility of any body is *independent* of the electrostatic boundary conditions obeyed at the solid/fluid interface.

From a microfluidic standpoint, however, the induced non-uniformity in the zeta potential of a conducting or polarizable surface gives rise to a host of interesting phenomena, which to our knowledge have not yet been explored. Furthermore, the resulting phenomena affect the assumptions which underlie the classic results of Morrison(1970) and thus have important implications for electrophoresis of typical (dielectric) particles as well as fundamental colloidal science itself.

### 1.2. Induced-charge electro-osmosis

In this article, we build on the work of Bazant & Squires (2003), introducing and analyzing 'induced-charge electro-osmosis' (ICEO), the general phenomenon of electro-osmotic flow driven by an applied field acting on non-equilibrium, inhomogeneous charge clouds

induced at polarizable surfaces, such as conductors or dielectrics. Because the effect is nonlinear in the applied field, it can be used to drive steady electrokinetic flows using AC fields, as well as DC fields. The nonlinearity also allows for much larger fluid velocities and much richer, geometry-dependent flow structure. These properties are in stark contrast to standard, ‘fixed-charge’ electro-osmosis, which, *e.g.*, gives zero time-averaged flow in an AC field.

We first review some recent studies of AC electrokinetic phenomena near electrodes. In the context of colloidal self-assembly, Trau *et al.*(1997) and Yeh *et al.*(1997) demonstrated that colloidal spheres can spontaneously self-assemble into crystalline aggregates near electrodes under AC applied fields. They proposed somewhat similar electrohydrodynamic mechanisms for this aggregation, in which an inhomogeneous screening cloud, is formed by (and interacts with) the inhomogeneous applied electric field (perturbed by the sphere), resulting in a rectified electro-osmotic flow directed radially in toward the sphere. More recently, Nadal *et al.*(2002) performed detailed measurements in order to test both the attractive (electrohydrodynamic) and repulsive (electrostatic) interactions between the spheres.

Steady electro-osmotic flows have also recently been achieved using AC electric fields. Ramos *et al.*(1999) theoretically and experimentally explored ‘AC electro-osmosis’, in which a pair of adjacent, flat electrodes located on a glass slide and subjected to AC driving, gives rise to a steady electro-osmotic flow consisting of two counter-rotating rolls. Around the same time, Ajdari(2000) theoretically predicted and Brown *et al.*(2000) experimentally demonstrated, that an asymmetric array of electrodes with applied AC fields generally pumps fluid in the direction of broken symmetry (‘AC pumping’). These effects, however, seem to only occur at electrodes, where the voltage is oscillated at a special AC frequency (the inverse of the charging time discussed below).

The present work complements, extends, and generalizes that of Trau *et al.*(1997), Yeh *et al.*(1997), Ramos *et al.*(1999), and Ajdari(2000), all of which rely upon the formation of inhomogeneous induced charge clouds. In these studies, the flows occur around electrodes, whose potential is deliberately driven at a certain frequency. We present here a considerably more general physical picture, demonstrating that ICEO flows can also occur around ‘inert’ conducting or polarizable surfaces that are electrically isolated from the driving electrodes, and can be driven by applied DC fields as well as AC or more general time-dependent fields. During writing of this article, Thamida & Chang(2002) have observed and modeled another special case of what we are calling ICEO, in which a nonlinear electrokinetic jet streams away from a dielectric corner/wedge under an applied DC electric field. This very recent experiment and those cited above on AC colloidal aggregation and microfluidic pumping demonstrate the remarkably broad applicability of ICEO.

Before we begin, we note the difference between ICEO and ‘electrokinetic phenomena of the second kind’, reviewed by Dukhin(1991) and studied recently by Ben & Chang(2002) with an eye towards microfluidic applications. Electrokinetic phenomena of the second kind typically occur around ion-selective porous granules subject to applied fields large enough to generate strong currents of certain ions through the liquid/solid interface. This leads to large concentration variations and space charge in the bulk electrolyte on one side, which interact with the applied field to cause motion. In principle, the same effect could also occur at non-porous electrode surfaces undergoing electrochemical reactions at very large Faradaic currents (exceeding diffusion limitation). In contrast, however, ICEO typically occurs at an inert polarizable surface (metal or dielectric) carrying no Faradaic current in a homogeneous, quasi-neutral bulk electrolyte and relies on relatively small

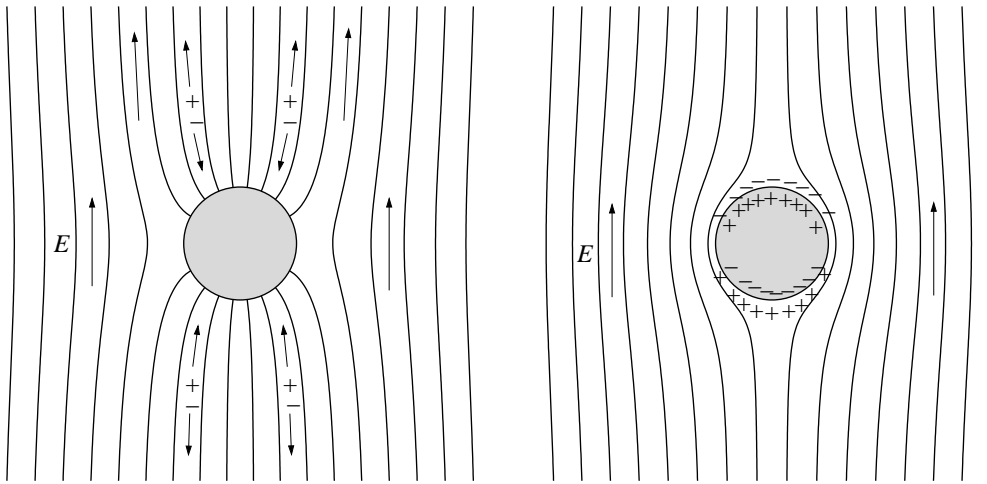


FIGURE 2. The evolution of the electric field around a solid conducting cylinder immersed in a liquid electrolyte, following the imposition of a background DC field at  $t = 0$  (a), where the field lines intersect normal to the conducting surface. Over a charging time  $\tau_c = \lambda_D a / D_i$ , a dipolar charge cloud forms in response to currents from the bulk, reaching steady state (b) when the bulk field profile is that of an insulator. The resulting zeta potential, however, is nonuniform.

induced double-layer charges, rather than bulk space charge. (Note that ICEO could occur as an additional effect in cases of second-kind electro-osmosis, but not vice versa.)

The article is organized as follows: Section 2 develops a basic physical picture of induced-charge electro-osmosis via calculations of steady ICEO flow around a conducting cylinder. Section 3 examines the time-dependent ICEO flow for background electric fields which are suddenly-applied (3.1) or sinusoidal (3.2). Section 4 describes some basic issues for ICEO in microfluidic devices, such as coupling to the external circuit, as well as the phenomenon of fixed-potential ICEO. Section 5 investigates the detrimental effect of a thin dielectric coating on the conductor surface and shows the ICEO also occurs for non-conducting dielectric objects. Section 6 gives a systematic derivation of ICEO, starting with the basic electrostatic, fluid, and ion transport equations and employing a matched asymptotic expansion, concluding with a set of effective equations (with approximations and errors quantified) for the ICEO flow around an arbitrarily-shaped particle in an arbitrary space- and time-dependent electric field. The interesting consequences of shape and field asymmetries, which generally lead to electro-osmotic pumping or electrophoretic motion in AC fields, will be considered in a companion paper.

## 2. Induced-charge electro-osmosis: fundamental picture

Before delving into a systematic analysis of ICEO, it is instructive to begin with a simple example which can be analyzed in an intuitive fashion to illustrate the basic theory. This section is designed to give a physically clear (as well as quantitatively accurate) sense of ICEO in perhaps the simplest case. A systematic and general analysis, justifying the approximations made used here, appears in section 6.

### 2.1. Qualitative description

The basic phenomenon of induced charge electro-osmosis is illustrated in Figures 2 and 3. Immediately after an external field  $\mathbf{E} = E_0 \hat{\mathbf{z}}$  is applied, an initial electric field is set

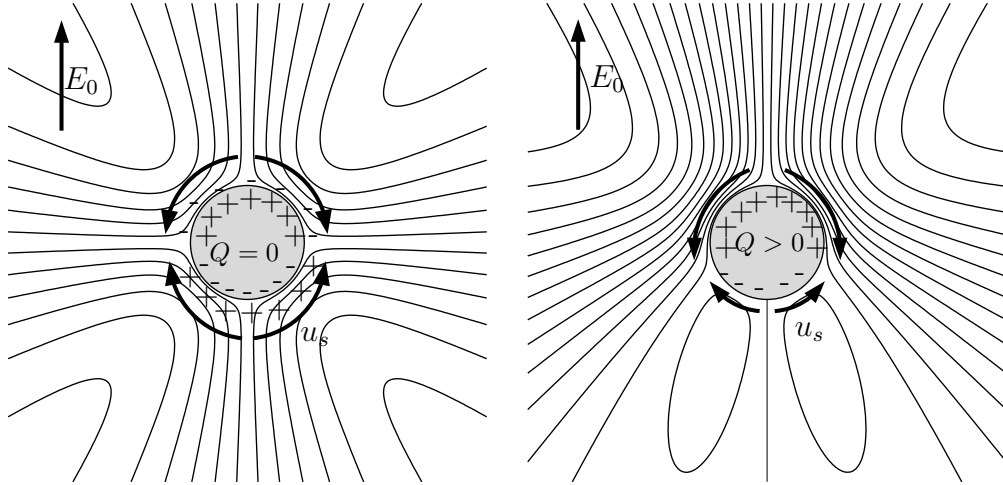


FIGURE 3. The steady-state induced-charge electro-osmotic flow around (a) a conducting cylinder with zero net charge and (b) a positively charged conducting cylinder.

up so that field lines intersect a conducting surface at right angles (figure 2a). If the conductor were in vacuum, this would represent the steady-state field configuration. In an electrolytic solution, however, mobile ions in solution move in response to applied fields, and a current  $\mathbf{j} = \sigma\mathbf{E}$  drives positive ions into a charge cloud on one side of the conductor ( $z < 0$ ), and negative ions to the other ( $z > 0$ ), and an opposite charge on the conducting surface is induced to maintain the equipotential surface. A dipolar charge cloud thus develops, charging until no field lines penetrate the double-layer in steady state (Figure 2b). In steady state, the tangential field  $E_{||}$  drives an electro-osmotic slip velocity (Eq. 1.4) proportional to the local double-layer charge density, driving fluid from the ‘poles’ of the particle towards the ‘equator’ (Figure 3a). The same flow can be driven using an AC field, as can be seen by the fact an oppositely-directed field induces an oppositely-charged screening cloud, so that the net flow (dependent on the product of the field and the charge) remains the same.

While we have specifically considered a conducting cylinder, a similar picture clearly holds for more general shapes. Below, we present calculations for cylinders in steady and unsteady applied fields and quote analogous results for spheres in Table 1. More generally, ICEO slip velocities around arbitrarily-shaped inert objects in uniform applied fields are directed along the surface from the ‘poles’ of the object (as defined by the applied field), towards the object’s ‘equator’.

## 2.2. Steady ICEO around an uncharged conducting cylinder

We consider an isolated, uncharged conducting cylinder of radius  $a$  submerged in an electrolyte solution with very small screening length  $\lambda_D \ll a$ . An external electric field  $E_0\hat{\mathbf{z}}$  is suddenly applied at  $t = 0$ , and after an extremely fast electronic relaxation time, charges within the conductor arrange themselves so that the conducting surface forms an equipotential surface, giving a potential

$$\phi_0 = -E_0 z \left(1 - \frac{a^2}{r^2}\right). \quad (2.1)$$

Electric field lines intersect the conducting surface at right angles, as shown in Figure 2a.

Were the cylinder in vacuum, Eq. (2.1) would represent the steady-state electric field. However, the electrolyte solution contains mobile ions which move in response to the electric field. Positive ions are driven in the direction of the local field, and negative ions in the direction opposite to that of the field. Due to the non-zero electrolyte conductivity  $\sigma$ , a non-zero current

$$\mathbf{j} = \sigma \mathbf{E} \quad (2.2)$$

is driven along field lines, and thus ions are transported up to the cylinder surface. In the absence of electrochemical reactions at the conductor/electrolyte interface (*i.e.* sufficiently low potentials that the cylinder is ‘ideally polarizable’), mobile solute ions accumulate in a screening cloud adjacent to the solid/liquid surface, attracting equal and opposite ‘image charges’ within the conducting cylinder itself. Thus the conductor’s surface charge density  $q$  — induced by the growing screening cloud — changes in a time-dependent fashion, via

$$\frac{dq(\theta)}{dt} = -j_{\perp} = \sigma \mathbf{E} \cdot \hat{\mathbf{r}}. \quad (2.3)$$

Using the approximate linear relationship (1.2) between surface charge density and zeta potential, this can be expressed as

$$\frac{d\zeta(\theta)}{dt} = \frac{\sigma}{\epsilon_w \kappa} \mathbf{E} \cdot \hat{\mathbf{r}}. \quad (2.4)$$

A dipolar charge cloud grows, since positively-charged ions are driven into the charge cloud on the side of the conductor nearest the field source ( $z < 0$  in this case), and negatively-charged ions are driven into the charge cloud on the opposite side. As ions are driven into the screening charge cloud, field lines are expelled, thereby reducing the ionic flux into the charge cloud.

The system reaches a steady state configuration when all field lines are expelled ( $\hat{\mathbf{r}} \cdot \mathbf{E}(a) = 0$ ). This occurs when the electrostatic potential outside of the charge cloud is given by

$$\phi_f = -E_0 z \left( 1 + \frac{a^2}{r^2} \right), \quad (2.5)$$

shown in Figure 2b. The steady-state electrostatic configuration is thus equivalent to the no-flux electrostatic boundary condition assumed in the analysis of ‘standard’ electrophoresis. In the present case, however, the steady-state configuration corresponds to a cylinder whose zeta potential varies with position according to

$$\zeta(\theta) = \phi_o - \phi_f(a) = 2E_0 a \cos \theta. \quad (2.6)$$

where the conductor’s potential vanishes,  $\phi_o = 0$ , by symmetry. While the steady-state electric field has no component normal to the charge cloud, it does have a non-zero tangential component, given by

$$\hat{\theta} \cdot \mathbf{E} = -2E_0 \sin \theta. \quad (2.7)$$

This tangential field drives an induced-charge electro-osmotic flow, with slip velocity given by equation (1.4), where the (spatially-varying) surface potential  $\zeta$  is now given by equation (2.6). Because the charge cloud is itself dipolar, the tangential field drives the two sides of the charge cloud in opposite directions—each side away from the poles—resulting in a quadrupolar electro-osmotic slip velocity

$$\mathbf{u}_s = 2U_0 \sin 2\theta \hat{\theta} \quad (2.8)$$

where  $U_0$  is the natural velocity scale for ICEO,

$$U_0 = \frac{\epsilon_w E_0^2 a}{\eta}. \quad (2.9)$$

One power of  $E_0$  sets up the ‘induced-charge’ screening cloud, and the second drives the resultant electro-osmotic flow.

The fluid motion in this problem is reminiscent of that around a fluid drop of one conductivity immersed in a fluid of another conductivity subjected to an external electric field, studied by Taylor(1966). By analogy, we find the radial and azimuthal fluid velocity components of the fluid flow outside of the cylinder to be

$$u_r = 2 \frac{a(a^2 - r^2)}{r^3} U_0 \cos 2\theta \quad (2.10)$$

$$u_\theta = 2 \frac{a^3}{r^3} U_0 \sin 2\theta. \quad (2.11)$$

Analogous results can be derived for the steady-state ICEO flow around a sphere, and are given in Table 1. Although we have focused on the analytically tractable case of linear screening in this paper, equations (2.10-2.11) for the steady-state ICEO flow around a conducting cylinder hold for non-linear screening as well.

### 2.3. Steady ICEO around a charged conducting cylinder

Until now, we have assumed the cylinder to have zero net charge for simplicity. A cylinder with non-zero equilibrium charge density  $q_0 = Q/4\pi a^2$ , or equivalent zeta potential

$$\zeta_0 = \epsilon_w \kappa q_0, \quad (2.12)$$

sets up a steady-state electro-osmotic slip which is a superposition of the ‘standard’ electro-osmotic flow due to the equilibrium zeta potential  $\zeta_0$ ,

$$\mathbf{u}_s^Q = \mathbf{u}_s - 2 \frac{\epsilon_w \zeta_0}{\eta} \sin \theta \hat{\theta} \quad (2.13)$$

where  $\mathbf{u}_s$  is the ICEO slip velocity, given in equation 2.8. The bulk flow is simply given by a superposition of the ICEO flow and the ‘standard’ electro-osmotic flow, and is shown in figure 3b.

The electrophoretic velocity of a charged conducting cylinder can be simply found using the results of Stone & Samuel(1996), who demonstrated that the velocity of a cylinder with prescribed slip velocity  $\mathbf{u}_s(\theta)$ , but no externally-applied force, is given by the surface-averaged velocity,

$$\mathbf{U} = \frac{1}{2\pi} \int_0^{2\pi} \mathbf{u}_s(\theta) d\theta. \quad (2.14)$$

The ICEO slip velocity (2.8) has zero surface average, as pointed out by Levich(1962), leaving only the ‘standard’ electro-osmotic slip velocity (2.13). This gives the usual electrophoretic mobility  $\mu_e = \epsilon_w \zeta_0 / \eta$ , for an object of fixed uniform charge density and constant zeta potential, which nicely illustrates the result of O’Brien & White(1978) that the mobility (linear response) does not depend on electrostatic boundary conditions, even though the flow around the particle clearly does.

## 3. Time-dependent ICEO

A significant feature of induced-charge electro-osmotic flow is its dependence on the square of the electric field. This has important consequences for AC fields: if the direction

	Cylinder	Sphere
Initial potential $\phi_i$	$-E_0 z \left(1 - \frac{a^2}{r^2}\right)$	$-E_0 z \left(1 - \frac{a^3}{r^3}\right)$
Steady-state potential $\phi_s$	$-E_0 z \left(1 + \frac{a^2}{r^2}\right)$	$-E_0 z \left(1 + \frac{a^3}{2r^3}\right)$
Steady-state zeta potential $\zeta$	$2E_0 a \cos \theta$	$\frac{3}{2}E_0 a \cos \theta$
Stream function $\psi$	$U_0 a \sin 2\theta \left(\frac{a^2}{r^2} - 1\right)$	$\frac{9}{8}U_0 a^2 \sin^2 \theta \cos \theta \left(\frac{a^2}{r^2} - 1\right)$
Radial flow $u_r$	$\frac{2a(a^2 - r^2)}{r^3} U_0 \cos 2\theta$	$\frac{9a^2(a^2 - r^2)}{16r^4} U_0 (1 + 3 \cos 2\theta)$
Azimuthal flow $u_\theta$	$\frac{2a^3}{r^3} U_0 \sin 2\theta$	$\frac{9a^4}{8r^4} U_0 \sin 2\theta$
Charging Timescale	$\tau_c = \frac{\lambda_D a}{D}$	$\tau_s = \frac{\lambda_D a}{D}$
Induced dipole strength: $g(t)$ for suddenly applied field $\mathbf{E}_0$	$g(t) = 1 - 2e^{-t/\tau_c}$	$g(t) = \frac{1}{2} (1 - 3e^{-2t/\tau_s})$
$g$ for AC field $\Re(\mathbf{E}_0 e^{i\omega t})$	$g = \frac{1 - i\omega\tau_c}{1 + i\omega\tau_c}$	$g = \frac{1 - i\omega\tau_s}{2 + i\omega\tau_s}$

TABLE 1. Electrostatic and hydrodynamic quantities for the induced-charge electro-osmotic (ICEO) flow around conducting spheres and cylinders, each of radius  $a$ . Here  $U_0 = \epsilon_w E_0^2 a / \eta$  is a characteristic velocity scale, and induced dipole strengths  $g$  are defined in equations (3.1) and (3.10).

of the electric field in the above picture is reversed, so are the signs of the induced surface charge and screening cloud. The resultant ICEO flow, however, remains unchanged: the net flow generically occurs away from the poles, and towards the equator. Therefore, induced-charge electro-osmotic flows persist even in an AC applied fields, so long as the frequency is sufficiently low that the induced-charge screening clouds have time to form.

It is thus of interest to examine the time-dependence of induced-charge electro-osmotic flows. As above, we explicitly consider a conducting cylinder, and simply cite the analogous results for conducting sphere in Table 1. While we conduct our analysis for the analytically-tractable case of linear screening, the approach can be extended to higher induced zeta potentials in a straightforward fashion. Two situations of interest are presented: the time-dependent response of a conducting cylinder to 1) a suddenly-applied electric field and 2) a sinusoidal AC electric field.

### 3.1. ICEO around a conducting cylinder in a suddenly-applied DC field

Consider first the time-dependent response of an uncharged conducting cylinder in an electrolyte when a uniform electric field  $\mathbf{E} = E_0 \hat{\mathbf{z}}$  is suddenly turned on at  $t = 0$ . The

dipolar nature of the external driving suggests a bulk electric field of the form

$$\phi(\mathbf{r}, t) = -E_0 z \left( 1 + g(t) \frac{a^2}{r^2} \right), \quad (3.1)$$

so that initially  $g(0) = -1$  (equation 2.1), and in steady state  $g(t \rightarrow \infty) = 1$  (equation 2.5). The potential of the conducting surface itself remains zero, so that the potential drop across the double layer is given by

$$\phi(a, \theta, t) = -\zeta(\theta) = -\frac{q(\theta)}{\epsilon_w \kappa}. \quad (3.2)$$

Here, as before, we take  $q$  to represent the induced surface charge, so that the total charge per unit area in the charge cloud is  $-q$ . The electric field normal to the surface, found from equation 3.1, drives an ionic current

$$j_{\perp} = -\dot{q}(\theta) = -\sigma E_0 \cos \theta (1 - g), \quad (3.3)$$

into the charge cloud, locally injecting a surface charge density  $\dot{q}$  per unit time. We express the induced charge density  $q$  in terms of the induced dipole  $g$  by substituting 3.1 into 3.2, take a time derivative, and equate the result with  $\dot{q}$  given by 3.3. This results in an ordinary differential equation for the dipole strength  $g$ ,

$$\dot{g} = \frac{\sigma}{\epsilon_w \kappa a} (1 - g), \quad (3.4)$$

whose solution is

$$g(t) = 1 - 2e^{-t/\tau_c}. \quad (3.5)$$

Here  $\tau_c$  is the characteristic time for the formation of the induced-charge screening clouds

$$\tau_c = \frac{\kappa a \epsilon_w}{\sigma} = \frac{\lambda_D a}{D}, \quad (3.6)$$

where the definitions of conductivity ( $\sigma = 2n_0 e^2 D / k_B T$ ) and screening length (1.3) have been used. The peculiar ‘mixed’ nature of this time scale, involving both length scales  $\lambda_D$  and  $a$ , is emphasized by Ajdari, Bazant & Thornton (2003) in their study of time-dependent electrode charging.

The induced-charge screening cloud (with equivalent zeta potential given by equation 3.2) is driven by the tangential field (derived from equation 3.1) in the standard way (equation 1.4), resulting in an induced-charge electro-osmotic slip velocity

$$\mathbf{u}_s = \frac{2\epsilon_w E_0^2 a}{\eta} \sin 2\theta \left( 1 - e^{-t/\tau_c} \right)^2 \hat{\theta}. \quad (3.7)$$

More generally, the time-dependent slip velocity around a cylinder with a nonzero fixed charge (or equilibrium zeta potential  $\zeta_0$ ) can be found in similar fashion, and results in the standard ICEO slip velocity  $\mathbf{u}_s$  (equation 3.7) with an additional term representing standard electro-osmotic slip (Eq. 2.13)

$$\mathbf{u}_s^Q = \mathbf{u}_s - 2 \frac{\epsilon_w \zeta_0}{\eta} \sin \theta \left( 1 - e^{-t/\tau_c} \right) \hat{\theta}. \quad (3.8)$$

Note that equation 3.8 grows more quickly than equation 3.7 initially, but that ICEO slip eventually dominates in strong fields, since it varies with  $E_0^2$ , versus  $E_0$  for the standard electro-osmotic slip.

Finally, we mention nonlinear screening effects. Although the equations are no longer analytically tractable, the analysis of this section can be generalized to account for various models of nonlinear screening, as developed by Bazant & Squires (2003). Typically,

the differential capacitance,  $|dq/d\zeta|$ , increases with  $|\zeta|$ , so qualitatively the poles of the cylinder along the applied field will charge more slowly than the sides perpendicular to the field, although the eventual steady-state field is always the same as in the case of linear screening.

### 3.2. ICEO around a conducting cylinder in a sinusoidal AC field

A similar calculation can be performed for sinusoidal applied fields. We represent the electric field using complex notation

$$\mathbf{E} = E_0 e^{i\omega t} \hat{\mathbf{z}}, \quad (3.9)$$

where the real part is implied, and assume a bulk electrostatic potential of the form

$$\phi(\mathbf{r}, t) = -E_0 z e^{i\omega t} \left( 1 + g \frac{a^2}{r^2} \right). \quad (3.10)$$

The perpendicular field drives a current into the charge cloud, injecting a charge density

$$\dot{q} = -\sigma E_0 e^{i\omega t} \cos \theta (1 - g), \quad (3.11)$$

per unit time. This injected charge density in turn determines the potential just outside the charge cloud via 3.2, giving

$$q = -\epsilon_w \kappa E_0 a \cos \theta e^{i\omega t} (1 + g) \quad (3.12)$$

Combining equations 3.11 and 3.12 gives a double-layer response

$$g = \frac{1 - i\omega\tau_c}{1 + i\omega\tau_c}, \quad (3.13)$$

for a time-dependent zeta potential

$$\zeta = 2E_0 a \cos \theta \Re \left( \frac{e^{i\omega t}}{1 + i\omega\tau_c} \right). \quad (3.14)$$

The resulting induced-charge electro-osmotic slip velocity is found to be

$$\mathbf{u}_s = \frac{2\epsilon_w E_0^2 a}{\eta} \sin 2\theta \left[ \Re \left( \frac{e^{i\omega t}}{1 + i\omega\tau_c} \right) \right]^2 \hat{\theta}, \quad (3.15)$$

with time-averaged slip velocity

$$\langle \mathbf{u}_s \rangle = \frac{\epsilon_w E_0^2 a \sin 2\theta}{\eta(1 + \omega^2 \tau_c^2)} \hat{\theta}. \quad (3.16)$$

In the low-frequency limit  $\omega\tau_c \ll 1$ , the double-layer fully develops in phase with the applied field. In the high-frequency limit  $\omega\tau_c \gg 1$ , the double-layer does not have time to charge up, attaining a maximum magnitude  $\sim 1/(\omega\tau_c)^2$  with a  $\pi/2$  phase shift.

## 4. ICEO in microfluidic devices

In the examples above, we have considered isolated conductors in background applied fields ‘at infinity’, but the remarkable richness of ICEO phenomena becomes more apparent when considering finite-size geometrical effects and electrical couplings in real microfluidic devices, as illustrated by two simple examples in this section. A more thorough discussion of microfluidic applications of ICEO will be presented elsewhere.

#### 4.1. Electrode screening

As emphasized above, applying an electric field,  $E_0(t)$ , in an homogeneous electrolyte really means applying a current,  $J_0(t) = \sigma E_0(t)$ . In electro-microfluidic devices, it is desirable to avoid persistent Faradaic currents because the associated electrochemical reactions may cause fluid contamination by reaction products or electrodeposits, unwanted concentration polarization, or permanent dissolution (and thus irreversible failure) of microelectrodes. Therefore, it is preferable to use oscillating voltages and non-Faradaic displacement currents at inert non-reactive electrodes. In that case, however, one must also consider the effect of diffuse-layer charging at the electrodes. Ajdari, Bazant & Thornton (2003) discuss electrode screening in detail, including both large applied potentials  $V_0 \gg k_B T/e$  and long screening lengths  $\lambda_D \approx L$ .

We examine the simplest case here, which involves a device consisting of a thin conducting cylinder of radius  $a \gg \lambda_D$  placed between flat, inert electrodes separated by  $2L \gg 2a$ . The cylinder is electrically isolated from the rest of the system, so that its total charge is fixed. In a suddenly applied DC voltage,  $2V_0$ , the bulk electric field,  $E_0(t)$ , decays to zero as screening clouds develop at the electrodes. For weak potentials ( $V_0 \ll k_B T/e$ ) and thin double-layers ( $\lambda_D \ll a \ll L$ ), the bulk field decays exponentially

$$E_0(t) = \frac{V_0}{L} e^{-t/\tau_e}, \quad (4.1)$$

with a characteristic electrode charging time

$$\tau_e = \frac{\lambda_D L}{D}, \quad (4.2)$$

analogous to the cylinder's charging time (equation 3.6). This time-dependent field  $E_0(t)$  then acts as the 'applied field at infinity' in the ICEO slip formula, Eq. (3.7).

Therefore, the basic picture is that the ICEO flow around the cylinder (including any net pumping in the case of nonzero total charge) is set into motion exponentially over the time scale,  $\tau_c = \lambda_D a / D$ , while it is terminated exponentially over a longer time scale,  $\tau_e = \lambda_D L / D$ , as the bulk field is screened at the electrodes. This interplay between two time scales, one set by the geometry of the driving surface and another set by the electrode geometry, is a common feature of ICEO in microfluidic devices.

This is clearly seen in the important case of AC forcing by a voltage,  $V_0 \cos(\omega t)$ . In that case, the bulk electric field is given by

$$E_0(t) = \frac{V_0}{L} \Re \left( \frac{i\omega\tau_e}{1 + i\omega\tau_e} e^{-i\omega t} \right). \quad (4.3)$$

Once again, electric fields persist in the bulk solution when the driving frequency is high enough ( $\omega\tau_e \gg 1$ ) that screening clouds do not have time to develop near the electrodes. Induced-charge electro-osmotic flows driven by applied AC fields can thus persist only in a certain band of driving frequencies,  $\tau_e^{-1} \leq \omega \leq \tau_c^{-1}$ , unless Faradaic reactions occur at the electrodes to maintain the bulk field. In the case of 'AC electro-osmosis' at adjacent surface electrodes studied by Ramos *et al.* (1999) and Ajdari (2000), these two time scales coincide to yield a single characteristic frequency for ICEO flow,  $\omega_c = 1/\tau_e$ .

Table 2 presents typical values for induced-charge electro-osmotic flow velocities and charging time scales for some reasonable microfluidic parameters. For example, an applied electric field of strength 100 V/cm across an electrolyte containing a 10  $\mu\text{m}$  cylindrical post gives rise to an ICEO slip velocity of order 1 mm/s, with charging times  $\tau_c \sim 0.1$  ms and  $\tau_e = 0.1$  s.

---

Material properties of aqueous solution		
Dielectric constant	$\epsilon_w \approx 80\epsilon_0$	$7 \times 10^{-5}$ g cm/V <sup>2</sup> s <sup>2</sup>
Viscosity	$\eta$	$10^{-2}$ g/cm s
Ion Diffusivity	$D_i$	$10^{-5}$ cm <sup>2</sup> /s
Experimental Parameters		
Screening Length	$\lambda_D$	10 nm
Cylinder radius	$a$	10 $\mu$ m
Applied field	$E_0$	100 V/cm
Electrode Separation	$L$	1 cm
Characteristic Scales		
Slip velocity	$U_0 = \epsilon_w E_0^2 a / \eta$	0.7 mm/s
Cylinder charging time	$\tau_c = \lambda a / D_i$	$10^{-4}$ s
Electrode charging time	$\tau_e = \lambda L / D_i$	$10^{-1}$ s

---

TABLE 2. Representative values for induced-charge electro-osmosis in a simple microfluidic device.

---

#### 4.2. Fixed-potential ICEO

In the above examples, we have assumed a conducting element which is electrically isolated from the driving electrodes. In such situations, the total charge on the conducting surface is constrained. Another possibility involves fixing the potential of the conducting surface with respect to the potential of the driving electrodes, allowing charge to flow onto and off of the conductor in order to maintain this fixed potential. This ability to directly control the induced charge allows for a wide variety of microfluidic pumping strategies exploiting ICEO.

Perhaps the simplest example of fixed-potential ICEO involves a conducting cylinder of radius  $a$  which is held in place at a distance  $h$  from the nearest electrode. For simplicity, we will consider  $a \ll h$  and  $h \ll L$ . We take the cylinder to be held at some potential  $V_c$ , the nearest electrode to be held at  $V_0$ , the other electrode at  $V = 0$ , and assume the electrode charging time  $\tau_e$  to be long. In this case, the bulk field (unperturbed by the conducting cylinder) is given simply by  $E_0 = V_0/L$ , and the ‘background’ potential at the cylinder location is given by  $\phi(h) = V_0(1 - h/L)$ . In order to maintain a potential  $V_c$ , an average zeta potential

$$\zeta_i = V_c - V_0 \left( 1 - \frac{h}{L} \right) \quad (4.4)$$

is induced via a net transfer of charge per unit length of  $\lambda_i = 2\pi\epsilon_w\kappa a \zeta_i$ , along with an equally and oppositely charged screening cloud.

This induced screening cloud is driven by the tangential electric field (2.7) in the standard way, giving a fixed-potential ICEO flow with slip velocity

$$\mathbf{u}_s^{FP} = \mathbf{u}_s + 2\frac{\epsilon_w}{\eta} \frac{V_0}{L} \sin \theta \left( V_c - V_0 + \frac{V_0 h}{L} \right) \hat{\theta}, \quad (4.5)$$

where  $\mathbf{u}_s$  is the quadrupolar ‘fixed-total-charge’ ICEO flow  $\mathbf{u}_s$  from equations 2.8 and 2.9, with  $E_0 = V_0/L$ . Note that both the magnitude and direction of the flow can be controlled by changing the position  $h$  or the potential  $V_c$  of the conductor. If the cylinder

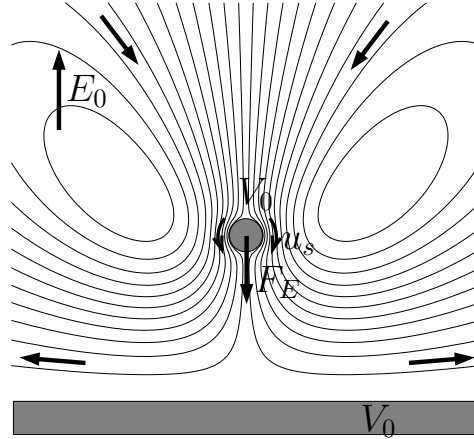


FIGURE 4. An example of fixed-potential ICEO. A cylinder of radius  $a$  is held a distance  $h \gg a$  from a nearby electrode and held at the same electrostatic potential  $V_0$  as the electrode. A second electrode (not shown) is located a distance  $L$  away and held at zero potential, so that a field  $E_0 \approx V_0/L$  is established. The background potential around the cylinder is  $V_0(1 - h/L)$ , so that a zeta-potential  $\zeta_i = V_0h/L$  is induced, with a charge transfer to the cylinder and an oppositely-charged screening cloud. If the cylinder were free to move, it would be electrophoretically driven away from the electrode with velocity  $U = \epsilon\epsilon_0 V_0^2 h / \eta L^2$ . The flow around the cylinder consists of the fixed-potential ICEO flow (source dipole flow) superposed with the flow driven by the force holding the cylinder in place (Stokeslet flow, with magnitude given by equation 4.7). The latter flow dominates in the far field. Like fixed-charge ICEO, a non-zero fixed-potential ICEO flow is driven even with an AC voltage.

were freely suspended, it would move with an electrophoretic velocity

$$U_E = \frac{\epsilon\epsilon_0}{\eta} \frac{V_0}{L} \left( V_c - V_0 + \frac{V_0 h}{L} \right) \quad (4.6)$$

away from the position  $h_c$ , where the unperturbed local potential  $V_0(1 - h_c/L)$  is equal to the fixed potential  $V_C$  of the cylinder.

On the other hand, if the cylinder were held in place against the electrophoretic velocity  $U_E$ , the force required to do so is given by Jeffrey & Onishi (1981) as

$$F_E = \frac{4\pi\eta U_E}{\log \left[ (h + \sqrt{h^2 - a^2})/a \right] - \sqrt{h^2 - a^2}/a} \approx \frac{4\pi\eta U_E}{\log(2h/a) - 1}, \quad (4.7)$$

and is directed toward  $h_c$ .

The fixed-potential ICEO flow around a cylinder held at the same potential as the nearest electrode ( $V_c = V_0$ , so that  $h_c = 0$ ) and held in place is shown in figure 4. Details of the leading-order bulk flow are briefly discussed in Appendix A. In this case, for an AC voltage,  $V_0 \cos(\omega t)$ , the time-averaged effective electrophoretic velocity is given by,

$$\langle U_E \rangle = \frac{\epsilon\epsilon_0 V_0^2 h}{2\eta L^2} = \frac{\epsilon\epsilon_0 h}{\eta} \langle E_0^2 \rangle, \quad (4.8)$$

which shows the same basic velocity scale as in the case of fixed-total-charge ICEO,  $U_0 = \epsilon\epsilon_0 E_0^2 a / \eta$ , with the size of the cylinder,  $a$ , replaced by the cylinder-electrode separation,  $h$ . Since typically  $h \gg a$ , we see that fixed-potential can lead to rather large microfluidic velocities, which vary nonlinearly with the applied voltage. These flows are also very sensitive to the device geometry and to the electrical coupling of the ‘working

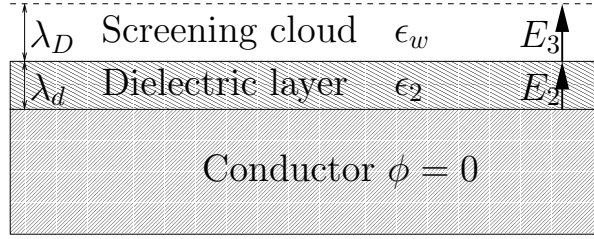


FIGURE 5. A dielectric layer of thickness  $\lambda_d$  and permittivity  $\epsilon_2$  coating a conductor. The potential drop between the external potential  $\phi_0$  and 0 at the conductor occurs in two steps:  $\Delta\phi_2 = E_2\lambda_d$  across the dielectric and  $\Delta\phi_3 \approx E_3\lambda_D$  across the double layer.

conductor' to the electrodes supplying the background driving field. (Note that in general, when no Faradaic current exists, there is little distinction between working conductors and electrodes since both impose voltages, undergo time-dependent screening, and may drive ICEO flows.) With all of this flexibility, it is clear that fixed-potential ICEO offers a powerful, additional technique to control the magnitude and spatial structure of microfluidic flows, in addition to fixed-total-charge ICEO.

### 5. Surface contamination by a dielectric coating

The above examples have focused on an idealized situation with a clean metal surface. In this section, we examine the effect of a non-conducting dielectric layer which coats the conductor, and find that any dielectric layer which is thicker than the screening length  $\lambda_D$  significantly reduces the strength of the ICEO flow. Furthermore, the ICEO flow around a dielectric object, rather than a perfectly conducting object as we have discussed so far, is presented as a limiting case of the analysis in this section.

We start with a simple physical picture to demonstrate the basic effect of a thin dielectric layer. Consider a conducting cylinder of radius  $a$  coated with a dielectric layer of thickness  $\lambda_d \ll a$  (so that the surface looks locally planar) and permeability  $\epsilon_2$ , as shown in Figure 5. In steady state, the potential drop from the conducting surface  $\phi = 0$  to the potential  $\phi_0$  outside of the double layer occurs across in two steps: across the dielectric (where  $E = E_2$ ), and across the screening cloud (where  $E = E_3$ ), so that

$$E_2\lambda_d + E_3\lambda_D = \phi_\infty. \quad (5.1)$$

The electric fields in the double layer and in the dielectric layer are related via  $\epsilon_2 E_2 = \epsilon_w E_3$ , so that

$$\left(1 + \frac{\epsilon_w}{\epsilon_2} \frac{\lambda_d}{\lambda_D}\right) E_3\lambda_D = \phi_\infty. \quad (5.2)$$

Since  $E_3\lambda_D$  is approximately the potential drop  $\zeta$  across the double-layer, and since the steady-state bulk potential is given by equation (2.5) to be  $\phi_\infty = 2E_0a \cos \theta$ , we find the induced-charge zeta potential to be

$$\zeta = \frac{2E_0a \cos \theta}{1 + \epsilon_w \lambda_d / \epsilon_2 \lambda_D}. \quad (5.3)$$

Thus unless the layer thickness  $\lambda_d$  is much less than  $\epsilon_2 \lambda_D / \epsilon_w$ , the bulk of the potential drop  $\phi_\infty$  occurs across the dielectric layer, instead of the double-layer, resulting in a reduced electro-osmotic slip velocity.

The modification to the charging time  $\tau_c$  for the coated cylinder can likewise be un-

derstood from this picture. The dielectric layer represents an additional (parallel-plate) capacitor of separation  $\lambda_d$  and filled with a dielectric  $\epsilon_2$ , in series with the capacitive screening cloud, giving a total capacitance

$$C_T = \frac{\epsilon_w}{\lambda_D} \left( 1 + \frac{\epsilon_w \lambda_d}{\epsilon_2 \lambda_D} \right)^{-1}, \quad (5.4)$$

and a modified RC time

$$\tau_c = \frac{\lambda_D a}{D} \left( 1 + \frac{\epsilon_w \lambda_d}{\epsilon_2 \lambda_D} \right)^{-1}. \quad (5.5)$$

A full calculation of the induced zeta potential around a dielectric cylinder of radius  $a$  coated by a dielectric layer with outer radius  $b$  and thickness  $(b - a)$  is straightforward although cumbersome, and is given in Appendix B. The resulting induced-charge zeta potential is

$$\zeta = \frac{2bE_0(1 + \Gamma_c) \cos \theta}{2 + \kappa b(1 - \Gamma_c)}, \quad (5.6)$$

with characteristic charging time scale

$$\tau_c = \frac{\lambda_D b}{D} \left[ 1 + \frac{\kappa b}{2}(1 - \Gamma_c) \right]^{-1}, \quad (5.7)$$

where  $\Gamma_c$  is defined to be

$$\Gamma_c = \frac{b^2 + a^2 - \epsilon_w/\epsilon_2(b^2 - a^2)}{b^2 + a^2 + \epsilon_w/\epsilon_2(b^2 - a^2)}. \quad (5.8)$$

It is instructive to examine limiting cases of the induced zeta potential (equation 5.6). In the limit of a ‘conducting’ dielectric coating  $\epsilon_2/\epsilon_w \rightarrow \infty$ , we recover the standard result for ICEO around a metal cylinder, as expected. In the limit of a thin dielectric layer  $b = a + \lambda_d$ , where  $\lambda_d \ll a$ , the induced zeta potential is given by

$$\zeta(\lambda_d \ll a) \approx \frac{2bE_0 \cos \theta}{1 + \lambda_d \epsilon_w / \lambda_D \epsilon_2}, \quad (5.9)$$

as found in equation 5.3, with a charging time

$$\tau_c(\lambda_d \ll a) \approx \frac{\lambda_D b}{D} \left( 1 + \frac{\epsilon_w \lambda_d}{\epsilon_2 \lambda_D} \right)^{-1}, \quad (5.10)$$

as found in equation 5.5. Therefore, the ICEO slip velocity around a coated cylinder is close to that of a clean conducting cylinder ( $\zeta = 2bE_0 \cos \theta$ ) only when the dielectric layer is much thinner than the screening length times the dielectric contrast,  $\lambda_d \ll \lambda_D \epsilon_2 / \epsilon_w$ . The zeta potential induced around a conducting cylinder with a thicker dielectric layer,

$$\zeta(\lambda_d \gg \lambda_D) \approx 2bE_0 \frac{\epsilon_2 \lambda_D}{\epsilon_w \lambda_d} \cos \theta, \quad (5.11)$$

is smaller by a factor of  $\mathcal{O}(\lambda_D / \lambda_d)$ , and the charging time,

$$\tau_c(\lambda_d \gg \lambda_D) \approx \frac{\epsilon_w \lambda_D}{\epsilon_2 \lambda_d} \frac{\lambda_D b}{D}, \quad (5.12)$$

is likewise shorter by a factor of  $\mathcal{O}(\lambda_D / \lambda_d)$ . As a result, strong ICEO flow requires a rather clean and highly polarizable surface, with minimal non-conducting deposits.

Note that the limit of a pure dielectric cylinder of radius  $b$  is found by taking the limit

$a \rightarrow 0$ . This gives a zeta potential of

$$\zeta(a=0) \rightarrow \frac{2bE_0 \cos \theta}{1 + \epsilon_w b / \epsilon_2 \lambda_D} \approx 2 \frac{\epsilon_2}{\epsilon_w} E_0 \lambda_D \cos \theta, \quad (5.13)$$

and an ICEO slip velocity which is smaller than the conducting case (2.8) by  $\mathcal{O}(\lambda_D/b)$ . The charging time for a dielectric cylinder is given by

$$\tau_c(a=0) \approx \frac{\epsilon_w \lambda_D^2}{\epsilon_2 D}, \quad (5.14)$$

as expected from equation 5.5 in the limit  $\lambda_d \gg \lambda_D$ .

## 6. Induced-charge electro-osmosis: systematic derivation

In this section, we follow the recent work of Bonnefont *et al.* (2001) and Ajdari, Bazant & Thornton (2003) on diffuse charge dynamics in order to systematically derive a set of effective equations for the time-dependent induced-charge electro-osmotic flow around an arbitrarily-shaped conducting object, and indicate the conditions under which the approximations made in this article are valid. Starting with the general equations for the electrostatic, fluid, and ion fields (as given by, *e.g.*, O'Brien & White (1978)), we propose an asymptotic expansion that matches an inner solution (valid within the charge cloud) with an outer region (outside of the charge cloud), and that accounts for two separated time scales—the time for the charge cloud to locally equilibrate and the time scale over which the external electric field changes. For simplicity, we perform the analysis for the case of a symmetric binary electrolyte.

The electrostatic field obeys Poisson's equation,

$$\nabla^2 \phi = -\frac{(n_+ - n_-)e}{\epsilon \epsilon_0}, \quad (6.1)$$

where  $n_{\pm}$  represent the local number density of positive and negative ions. The fluid flow obeys the Stokes equations, with body force given by the product of the charge density with the electric field,

$$\eta \nabla^2 \mathbf{u} - \nabla p = e(n_+ - n_-) \nabla \phi, \quad (6.2)$$

along with incompressibility. Finally, the ion field obeys the conservation equation

$$\frac{\partial n_{\pm}}{\partial t} + \nabla \cdot (n_{\pm} \mathbf{v}_{\pm}) = 0, \quad (6.3)$$

where  $\mathbf{v}_{\pm}$  represent the velocities of the two ion species,

$$\mathbf{v}_{\pm} = \mp b e \nabla \phi - k_B T b \nabla \log n_{\pm} + \mathbf{u}, \quad (6.4)$$

whose terms represent ion motion due to (a) electrostatic forcing, (b) diffusive motion down density gradients, and (c) advection with the local fluid velocity.

For boundary conditions on the surface  $\Gamma$  of the conductor, we require the fluid flow to obey the no-slip condition, the electric potential to be an equipotential, and the ions to obey a no-flux condition:

$$\mathbf{u}(\Gamma) = \mathbf{0} \quad (6.5)$$

$$\phi(\Gamma) = \zeta_0 \quad (6.6)$$

$$\mathbf{v}_{\pm}(\Gamma) \cdot \hat{\mathbf{n}} = 0, \quad (6.7)$$

where  $\hat{\mathbf{n}}$  represents the (outer) normal to the surface  $\Gamma$ .

Far from the object, we require the fluid flow to decay to zero, the electric field to approach the externally-applied electric field, and the ion densities  $n_{\pm}$  to approach their constant (bulk) value  $n_0$ . We therefore insert

$$n_+ = n_0 + p \quad (6.8)$$

$$n_- = n_0 + m, \quad (6.9)$$

and require that the excess positive and negative ion concentrations  $p$  and  $m$  decay far from the surface  $\Gamma$ .

In order to simplify these equations, we insert (6.4) in (6.3), and take the sum and difference of the resulting equations for the two ion species to obtain

$$\dot{c}^{\rho} + D\kappa^2 c^{\rho} - D\nabla^2 c^{\rho} - eb\nabla \cdot [c^e \nabla \phi] + \mathbf{u} \cdot \nabla c^{\rho} = 0 \quad (6.10)$$

$$\dot{c}^e - D\nabla^2 c^e - be\nabla \cdot [c^{\rho} \nabla \phi] + \mathbf{u} \cdot \nabla c^e = 0, \quad (6.11)$$

where we have used (6.1) and where we have defined

$$c^{\rho} = p - m \quad (6.12)$$

$$c^e = p + m. \quad (6.13)$$

The excess ion density ( $c^e = n_+ + n_- - 2n_0$ ) represents the local, charge neutral, excess ion concentration, whereas the difference ( $c^{\rho} = n_+ - n_-$ ) of ion densities is related to the net charge density via  $c^{\rho} = \rho/e$ . Both  $c^e$  and  $c^{\rho}$  must decay away from the solid surface, and obey the no-flux boundary conditions,

$$\frac{\partial c^{\rho}}{\partial n} \bigg|_{\Gamma} = -\frac{2n_0 e}{k_B T} \frac{\partial \phi}{\partial n} \bigg|_{\Gamma} - \frac{e}{k_B T} c^e \frac{\partial \phi}{\partial n} \bigg|_{\Gamma} \quad (6.14)$$

$$\frac{\partial c^e}{\partial n} \bigg|_{\Gamma} = -\frac{e}{k_B T} c^{\rho} \frac{\partial \phi}{\partial n} \bigg|_{\Gamma}, \quad (6.15)$$

at the surface  $\Gamma$ , where  $n$  denotes the coordinate which is locally normal to the surface.

In what follows, we solve the governing equations (6.1), (6.10), and (6.11), using a matched asymptotic expansion. We analyze first the solution in the ‘inner’ region within a distance of order  $\lambda_D$  of the surface. Non-dimensionalization yields a set of approximate equations for the inner region and a set of matching boundary conditions which depend on the ‘outer’ solution, valid in the quasi-neutral bulk region (farther than  $\lambda_D$  from the surface). Similarly, approximate equations and effective boundary conditions for the outer region are found. By solving the inner problem and matching to the outer problem, a set of effective equations are derived for bulk ICEO flows.

### 6.1. Non-dimensionalization: inner solution

We non-dimensionalize to determine the relative importance of terms in these equations, starting with the ‘inner’ solution, valid on the scale of the charge cloud. We assume the screening length to be much smaller than any length  $L$  associated with the surface, parametrized through

$$\epsilon = (\kappa L)^{-1} = \lambda_D/L \ll 1, \quad (6.16)$$

so that the screening cloud looks locally planar. We introduce a locally Cartesian coordinate system  $\{n, l\}$ , where  $n$  is locally normal to the surface, and  $l$  is locally tangent to the surface. We scale distances with the screening length  $\kappa^{-1}$ , and time with the diffusion time  $(\kappa^2 D)^{-1}$  appropriate for this distance. Since the potential is induced by an external field  $E_0$ , the natural scale for  $\phi$  is  $E_0 L$ , and the ICEO velocity scale is  $U_0 = \epsilon_w E_0^2 L / \eta$ .

We thus introduce the following scalings,

$$n = \kappa^{-1}\tilde{n}, \quad l = \kappa^{-1}\tilde{l}, \quad t = (\kappa^2 D)^{-1}\tilde{t}, \quad \phi = E_0 L \tilde{\phi}, \quad \mathbf{u} = U_0 \tilde{\mathbf{u}}. \quad (6.17)$$

Note that we scale time for the inner problem to the Debye time,  $\tau_D = (\kappa^2 D)^{-1} = \lambda_D^2/D$ , although the analysis may dictate another time scale (as expected from the physical arguments above).

We separate the electrostatic potential  $\tilde{\phi}$  into two components,

$$\tilde{\phi} = \tilde{\zeta} + \tilde{\psi}, \quad (6.18)$$

where  $\tilde{\zeta}(\tilde{n}, \epsilon \tilde{l})$  results from excess ionic charge in the screening cloud and decays to zero far from the body, and  $\tilde{\psi}(\epsilon \tilde{n}, \epsilon \tilde{l})$  satisfies Laplace's equation and varies on the macroscopic length scale  $L$ . Equation (6.1) then becomes

$$\tilde{\nabla}^2 \tilde{\zeta} = -\tilde{c}^\rho \quad (6.19)$$

$$\tilde{\nabla}^2 \tilde{\psi} = 0, \quad (6.20)$$

where we have used the natural scale for  $c^\rho$ ,

$$c_0^\rho = \frac{2n_0 e E_0 L}{k_B T}. \quad (6.21)$$

The equipotential boundary condition is given by

$$\tilde{\zeta}(\Gamma) + \tilde{\psi}(\Gamma) = \tilde{\zeta}_0, \quad (6.22)$$

where  $\tilde{\zeta}_0 = \zeta_0/(E_0 L)$  is the equilibrium zeta potential. With these definitions, the dimensionless ion conservation equations are

$$\frac{\partial \tilde{c}^\rho}{\partial \tilde{t}} + \tilde{c}^\rho - \tilde{\nabla}^2 \tilde{c}^\rho - \Psi^2 \tilde{\nabla} \cdot [\tilde{c}^e \tilde{\nabla} \tilde{\zeta}] - \Psi^2 \epsilon \tilde{\nabla} \cdot [\tilde{c}^e \tilde{\nabla} \tilde{\psi}] - P \tilde{\mathbf{u}} \cdot \tilde{\nabla} \tilde{c}^\rho = 0 \quad (6.23)$$

$$\frac{\partial \tilde{c}^e}{\partial \tilde{t}} + \tilde{\nabla}^2 \tilde{c}^e + \tilde{\nabla} \cdot [\tilde{c}^\rho \tilde{\nabla} \tilde{\zeta}] - \epsilon \tilde{\nabla} \cdot [\tilde{c}^\rho \tilde{\nabla} \tilde{\psi}] - P \tilde{\mathbf{u}} \cdot \tilde{\nabla} \tilde{c}^e = 0, \quad (6.24)$$

where we have introduced a dimensionless surface potential,

$$\Psi = \frac{e E_0 L}{k_B T}, \quad (6.25)$$

and Péclet number,

$$P = \frac{U_0}{\kappa D}, \quad (6.26)$$

and where the scale for  $c^e$  is taken to be

$$c_0^e = \Psi c_0^\rho \quad (6.27)$$

to satisfy the dominant balance in (6.24).

It is helpful to examine the physical significance of each of the terms in equation (6.23) individually. The first three terms give the dominant balance, and represent a (possible) transient, electrostatic transport, and diffusive transport, respectively. The next two terms represent the divergence of a flux of excess ionic concentration  $\tilde{c}^e$  (but not excess charge) due to an electric field set up by gradients in the charge cloud ( $\tilde{\nabla} \tilde{\zeta}$ ) or by the external field ( $\tilde{\nabla} \tilde{\psi}$ ). Both of these terms are small when the dimensionless surface potential  $\Psi$  is small—the regime within which the linearization of the Poisson-Boltzmann equation is valid. Furthermore, tangential variations in the electric and ion fields are assumed to occur on the macroscopic length scale  $L$ , so that these terms are  $\mathcal{O}(\epsilon^2)$ , even if the surface potential is not small. Thus ionic transport parallel to the surface, whether

due to an external tangential field, or to a field caused by a gradient in charge cloud strength, is typically small. The final term represents advection with the fluid flow  $\tilde{\mathbf{u}}$ .

The boundary conditions (6.14-6.15) in non-dimensional form are given by

$$\frac{\partial \tilde{c}^\rho}{\partial \tilde{n}} \Big|_\Gamma = - \left( \frac{\partial \tilde{\zeta}}{\partial \tilde{n}} + \epsilon \frac{\partial \tilde{\psi}}{\partial \tilde{n}} \right) \Big|_\Gamma [1 + \Psi^2 \tilde{c}^e] \Big|_\Gamma \quad (6.28)$$

$$\frac{\partial \tilde{c}^e}{\partial \tilde{n}} \Big|_\Gamma = - \left( \tilde{c}^\rho \frac{\partial \tilde{\zeta}}{\partial \tilde{n}} + \epsilon \frac{\partial \tilde{\psi}}{\partial \tilde{n}} \right) \Big|_\Gamma. \quad (6.29)$$

For small surface potentials  $\Psi \ll 1$ ,  $c^e$  is negligible compared to  $c^\rho$  (from equation 6.27), and the neglect of terms of order  $\mathcal{O}(\Psi^2, \epsilon \Psi^2)$  removes  $\tilde{c}^e$  from the equation (6.23) and boundary condition (6.28) for  $\tilde{c}^\rho$ .

### 6.2. Inner region: approximate solution

In what follows, we assume that the dimensionless surface potential  $\Psi$ , the Péclet number,  $P$ , and the dimensionless screening length  $\epsilon$ , are all small. The small surface potential (linear screening) limit,  $\Psi \ll 1$ , is taken for analytical convenience rather than necessity, and can be generalized, as discussed below. The regular limit of small Péclet number,  $P \ll 1$ , which holds in almost any situation, is easily taken by setting  $P = 0$ . The singular limit of thin double layers,  $\epsilon \ll 1$ , is the basis for using matched asymptotic expansions.

We expect the charge cloud  $\tilde{c}^\rho$  and electric potential  $\tilde{\zeta}$  to vary quickly in the  $n$ -direction, but slowly in the  $l$ -direction along the surface. Furthermore, we expect the charge cloud to exhibit two time scales: a fast (transient) time scale, over which  $\tilde{c}^\rho$  reaches a quasi-steady dominant balance, and a slow time scale  $1/\epsilon$ , over which the quasi-steady solution changes. The latter expectation is not obvious *a priori*, but it is informed by the physical arguments leading to the charging time (equation 3.6),  $\tau_c = \lambda_D L/D = \tau_D/\epsilon$ . It is also justified *a posteriori* by the successful asymptotic matching below, which selects this unique scaling as  $\epsilon \rightarrow 0$ .

Guided by these expectations, we propose ion densities of the form  $\tilde{c}^\rho(\tilde{n}, \epsilon l, \tilde{t}, \epsilon \tilde{t})$  and electric fields of the form  $\tilde{\zeta}(\tilde{n}, \epsilon l, \tilde{t}, \epsilon \tilde{t})$  and  $\tilde{\psi}(\epsilon \tilde{n}, \epsilon l, \tilde{t}, \epsilon \tilde{t})$ , resulting in governing equations

$$\dot{\tilde{c}}^\rho + \tilde{c}^\rho - \frac{\partial^2 \tilde{c}^\rho}{\partial \tilde{n}^2} = 0 + \mathcal{O}(\Psi^2, \epsilon \Psi^2, \epsilon^2, P) \quad (6.30)$$

$$\frac{\partial^2 \tilde{\zeta}}{\partial \tilde{n}^2} = -\tilde{c}^\rho + \mathcal{O}(\epsilon^2) \quad (6.31)$$

$$\tilde{\nabla}^2 \tilde{\psi} = 0 + \mathcal{O}(\epsilon^2). \quad (6.32)$$

The far-field boundary conditions for equations 6.30-6.32 are

$$\tilde{c}^\rho(\tilde{n} \rightarrow \infty) \rightarrow 0 \quad (6.33)$$

$$\tilde{\zeta}(\tilde{n} \rightarrow \infty) \rightarrow 0 \quad (6.34)$$

$$\left. \frac{\partial \tilde{\psi}}{\partial \tilde{n}} \right|_{\tilde{n} \rightarrow \infty} \rightarrow -\epsilon \tilde{E}_\perp(\epsilon l, \epsilon \tilde{t}), \quad (6.35)$$

where  $\tilde{E}_\perp = E_\perp/E_0$  is the normal component of the ‘outer’ (bulk) electric field at  $\Gamma$ . Because  $\tilde{\psi}$  varies only on the macroscopic length  $L$ , this ‘outer’ electric field does not vary across the inner region,

$$\left. \frac{\partial \tilde{\psi}}{\partial \tilde{n}} \right|_\Gamma = -\epsilon \tilde{E}_\perp + \mathcal{O}(\epsilon^2). \quad (6.36)$$

This gives equipotential and no-flux boundary conditions at the surface  $\Gamma$ ,

$$\tilde{\psi}(\Gamma) + \tilde{\zeta}(\Gamma) = \tilde{\zeta}_0 \quad (6.37)$$

$$\frac{\partial \tilde{c}^\rho}{\partial \tilde{n}} \Big|_\Gamma = - \frac{\partial \tilde{\zeta}}{\partial \tilde{n}} \Big|_\Gamma + \epsilon \tilde{E}_\perp + \mathcal{O}(\Psi^2). \quad (6.38)$$

In order to capture the long-time dynamics of the charge cloud, we pose an expansion for the quasi-steady distribution of  $\tilde{c}^\rho$  (and therefore  $\tilde{\zeta}$ ) of the form

$$\tilde{c}^\rho = \tilde{c}_0^\rho(\epsilon \tilde{l}, \tilde{n}, \epsilon \tilde{t}) + \epsilon \tilde{c}_1^\rho(\epsilon \tilde{l}, \tilde{n}, \epsilon \tilde{t}). \quad (6.39)$$

We have neglected the initial transient which occurs just after the field is applied and decays on times of  $\mathcal{O}(1)$ , choosing to focus on the long-time  $\sim 1/\epsilon$  behavior. Inserting the expansion (6.39) into the governing equations (6.30) and (6.31) results in a concentration field and potential

$$\tilde{c}^\rho = \tilde{c}_0^\rho e^{-\tilde{n}} - \epsilon \frac{\dot{\tilde{c}}_0^\rho}{2} \tilde{n} e^{-\tilde{n}} + \mathcal{O}(\epsilon^2) \quad (6.40)$$

$$\tilde{\zeta} = -\tilde{c}_0^\rho e^{-\tilde{n}} + \epsilon \frac{\dot{\tilde{c}}_0^\rho}{2} [2e^{-\tilde{n}} + \tilde{n} e^{-\tilde{n}}] + \mathcal{O}(\epsilon^2). \quad (6.41)$$

The fields  $\tilde{c}^\rho$  and  $\tilde{\zeta}$  are coupled through the boundary condition (6.38), giving

$$\dot{\tilde{c}}_0^\rho(\epsilon \tilde{t}) = -\epsilon \tilde{E}_\perp. \quad (6.42)$$

The factor of  $\epsilon$  shows that the correct time scale for charging dynamics is  $\tau_c/\epsilon = \lambda_D L/D$ , as claimed above.

Equation 6.42 can be recast in dimensional terms,

$$\dot{c}_0^\rho(\epsilon t) = -\frac{\kappa \sigma E_\perp}{e}, \quad (6.43)$$

giving an effective equation for the time-dependent zeta potential

$$\frac{\partial \zeta}{\partial t} = \frac{\sigma E_\perp}{\epsilon_w \epsilon_0 \kappa}, \quad (6.44)$$

reproducing equation (2.4). Lastly, we must solve for the electric field in the outer region to determine the normal field  $E_\perp$  at the surface, which determines the time derivative of the induced zeta potential via Eq. (6.44).

### 6.3. Outer solution and effective equations

Outside of the charge cloud, the charge density  $c^\rho$  and the field  $\zeta$  are exponentially small and thus neglected. All that remains is the bulk electrostatic field  $\psi$ , which satisfies Laplace's equation. We separate  $\psi$  into two components,

$$\psi = \psi_i + \psi_\infty, \quad (6.45)$$

where  $\psi_\infty$  is 'externally applied' (and therefore specified), and  $\psi_i$  is the perturbation induced by the object. We need to determine  $\psi_i$ , which obeys Laplace's equation

$$\nabla^2 \psi_i = 0, \quad (6.46)$$

subject to a decaying far-field boundary condition

$$\psi_i(|\mathbf{r}| \rightarrow \infty) \rightarrow 0, \quad (6.47)$$

and an equipotential condition on the surface  $\Gamma$ ,

$$\psi_i(\Gamma) = \zeta_0 - \psi_\infty(\Gamma) - \zeta(\Gamma, t). \quad (6.48)$$

If the induced zeta potential  $\zeta(\Gamma)$  is known at some time  $t$ , then equation 6.46 can be solved for the induced bulk potential  $\psi_i$  subject to the boundary conditions (6.47 and 6.48). From this, the normal field

$$E_\perp = -\hat{\mathbf{n}} \cdot \nabla(\psi_i + \psi_\infty)_\Gamma \quad (6.49)$$

can be found and used in Eq. (6.44) to calculate the time derivative of  $\zeta$  and close the system. In this fashion, the (time-dependent) induced zeta potential for an arbitrarily-shaped conducting surface immersed in an arbitrary time-dependent, spatially-varying electric field can be found without explicitly calculating the detailed structure of the screening cloud. Rather, one needs only solve for the bulk electric field (6.46) subject to a time-dependent boundary condition (6.48) whose time dependence is given by 6.44.

We have thus matched the bulk field outside the charge cloud with the ‘inner’ behavior of the charge cloud in a self-consistent manner. The ‘inner’ solutions for  $c^\rho$  and  $\zeta$  equilibrate quickly in response to the (slow) charging, and affect the boundary conditions which determine the ‘outer’ solution. The matching condition (6.44) results in a relation between the charge cloud and normal ionic flux, confirming the validity of equations (2.4), (3.3), and (3.11), which were previously argued in an intuitive, physical manner. This analysis has demonstrated that errors to this approach are of order  $\mathcal{O}(\Psi^2)$ ,  $\mathcal{O}(P)$  and  $\mathcal{O}(\epsilon^2)$ .

The full power of asymptotic analysis lies in its ability to handle the nonlinear regime of strong fields,  $\Psi = O(1)$ , as easily as the linear regime of weak fields discussed here. The net result is that Eq. (6.44) for linear charging is replaced by,

$$\frac{dq_D(\zeta)}{dt} = \sigma E_\perp, \quad (6.50)$$

where  $q_D(\zeta)$  is the total diffuse-layer charge density, generally a nonlinear function of the zeta potential, depending on the detailed model of the electrolyte/solid interface. The implications of this analysis for a general nonlinear theory of ICEO flows are summarized in Bazant & Squires (2003).

#### 6.4. ICEO fluid slip velocity

Lastly, we examine the ICEO slip velocity that results when the electric field  $-\nabla\phi$  drives the ions in the induced charge screening cloud  $c^\rho$ . The fluid flow obeys the unsteady Stokes equation

$$\rho \frac{\partial \mathbf{u}}{\partial t} = \eta \nabla^2 \mathbf{u} - \nabla p - \rho \nabla \phi. \quad (6.51)$$

along with incompressibility  $\nabla \cdot \mathbf{u} = 0$ .

We look first at the flow in the ‘inner’ region (diffuse double layer) of size  $\lambda_D$ , which approaches the ‘slip’ velocity (1.4) just outside the charge cloud. The curl of the unsteady Stokes equation gives a diffusion equation for vorticity,

$$\rho \frac{\partial \omega}{\partial t} = \eta \nabla^2 \omega, \quad (6.52)$$

from which it is seen that the time required for vorticity to diffuse a distance  $\lambda_D$  (and therefore for the ICEO slip velocity to reach steady state) is

$$\tau_\omega(\lambda_D) = \rho \lambda_D^2 / \eta, \quad (6.53)$$

which is very fast:  $\tau_\omega \approx 10^{-10}$  s for  $\lambda_D = 10$  nm. Thus the ICEO slip velocity in the inner region can be considered to follow changes in  $\zeta$  or  $\phi$  effectively instantaneously. Note, however, that in the bulk region the vorticity diffusion time is much longer,  $\tau_\omega(L) = \rho L^2/\eta = \tau_\omega(\lambda_D)/\epsilon^2$ , so the unsteady term in the Stokes equations may be important, especially at high AC frequencies.

Second, we demonstrate that the Helmholtz-Smoluchowski expression for the slip velocity (1.4) holds even for a spatially-varying zeta potential. We re-express the Stokes equations using a stream function  $\psi$ ,

$$\eta \nabla^4 \psi = \left( \frac{\partial \rho}{\partial n} \frac{\partial \phi}{\partial l} - \frac{\partial \rho}{\partial l} \frac{\partial \phi}{\partial n} \right) \quad (6.54)$$

and consider the ICEO flow above a conducting surface, driven by an applied tangential electric field  $E_{\parallel}$ . In steady state, the tangential field induces a gradient in charge cloud density, electrostatic potential, and zeta potential, given by

$$\rho = \rho_0 l e^{-\kappa n} \quad (6.55)$$

$$\phi = -E_{\parallel} l (1 - e^{-\kappa n}) \quad (6.56)$$

$$\zeta = E_{\parallel} l \quad (6.57)$$

where

$$\rho_0 = -\epsilon \epsilon_0 \kappa^2 E_{\parallel} \quad (6.58)$$

to satisfy Poisson's equation (6.1). One can verify that (6.54) is solved by

$$\psi = -\frac{\epsilon \epsilon_0 E_{\parallel}^2}{\kappa \eta} (l e^{-n} - l + \kappa l n), \quad (6.59)$$

from which the tangential and normal flows are calculated to be

$$u_l = \psi_n = -\frac{\epsilon \epsilon_0 E_0^2}{\mu} l (1 - e^{-\kappa n}) \rightarrow -\frac{\epsilon \epsilon_0 E_0^2 l}{\mu} \quad (6.60)$$

$$u_n = -\psi_l = -\frac{\epsilon \epsilon_0 E_0^2}{\mu} l \left( \frac{1 - \kappa n - e^{-\kappa n}}{\kappa} \right) \rightarrow -\frac{\epsilon \epsilon_0 E_0^2}{\mu} (\lambda_D - n). \quad (6.61)$$

On the charge-cloud scale  $n \sim \mathcal{O}(\lambda_D)$ , the tangential flow does indeed asymptote to equation (1.4) with a local zeta potential given by (6.57), and the normal flow velocity is smaller by a factor of order  $\mathcal{O}(\epsilon)$ .

In conclusion, an ICEO slip velocity is very rapidly established in response to an induced zeta potential and ‘outer’ tangential field. Despite the gradient in tangential field across the double layer and the gradients in induced zeta potential, the ICEO slip velocity is still given by the classical Helmholtz-Smoluchowski formula, Eq. (1.4). The bulk ICEO flow must then be found by solving the unsteady Stokes equations, with no forcing, but with a specified ICEO slip velocity on the boundary  $\Gamma$ , given by solving the effective electrochemical transport problem above.

## 7. Summary and Discussion

In this article, we have described the general phenomenon of induced-charge electro-osmosis (ICEO), which includes a wide variety of new techniques for driving a steady microfluidic flow around conducting or dielectric surfaces using AC or DC electric fields. We have given a physical picture of the basic mechanism for ICEO, involving the inhomogeneous surface charge induced in the conductor in order to maintain an equipotential

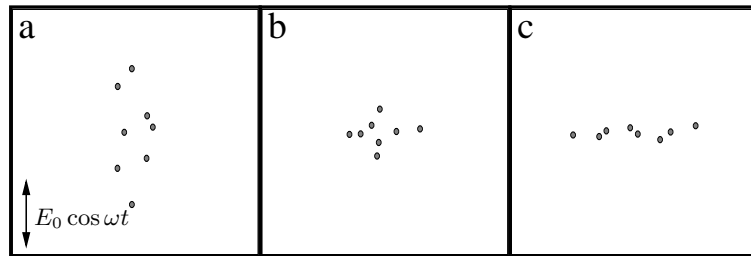


FIGURE 6. The evolution of a suspension of conducting colloidal particles moving electrophoretically due to an applied AC field. Particles would experience identically zero interaction in standard electrophoresis, and the suspension would simply translate with velocity  $\mu_e E_0 \cos \omega t$ . Induced-charge electro-osmotic flows, however, lead to non-zero time-averaged interactions that flatten the suspension into a ‘disk’ that spreads perpendicular to the applied field. This simulation accounts for particle advection in the leading order ICEO fluid flow (equations 2.9-2.11) set up around each particle.

surface in the presence of an applied field. In response, the electric field normal to the surface/charge cloud drives ions into an inhomogeneous (dipolar) charge cloud, which are in turn driven by the tangential electric field. This results in ICEO slip velocities of typical size  $U_0 \sim \epsilon_w E_0^2 a / \eta$ . A charging time scale  $\tau_c \sim \lambda_D a / D$  is required for these induced charge clouds to form. Due to the dependence on the square of the applied field  $E_0$ , a nonzero time-averaged ICEO flow can be driven using AC fields of sufficiently low frequencies ( $\omega \ll 1/\tau_c$ ).

We have performed explicit calculations for the steady and unsteady ICEO slip velocities (suddenly-applied and sinusoidal fields) around symmetric conducting cylinders. The ICEO flow is quadrupolar and decays with distance like  $\sim 1/r$  for conducting cylinders, and  $\sim 1/r^2$  for conducting spheres. We have also performed a systematic, matched-asymptotics analysis of the equations for the ion transport, electrostatics and fluid flow to confirm the validity of our physically intuitive approach. The analysis produces a set of effective equations which ‘integrate out’ the dynamics of the thin screening cloud, allowing the bulk ICEO flow to be calculated with macro-scale calculations alone.

We have also considered polarizable dielectric surfaces for two reasons. Firstly, we show that a dielectric layer of thickness  $\lambda_d$  can reduce the strength of the ICEO slip velocity by a factor of order  $\lambda_D/a$  when the dielectric layer is sufficiently thick ( $\lambda_d \gg \lambda_D$ ). This underscores the necessity of using clean and/or treated surfaces to ensure a clean conductor/water interface. Secondly, we show that an ICEO flow is set up even around a purely dielectric colloidal particle of permittivity  $\epsilon_2$ , but with reduced ICEO slip velocity,  $U_0 \sim \epsilon_2 E_0^2 \lambda_D / \eta$ .

These results have fundamental implications for electrophoresis in colloidal science. Morrison’s classic work on electrophoresis demonstrates that the electrostatic and hydrodynamic interactions between colloids exactly cancel each other during electrophoresis. This argument relies upon a zeta potential which is constant on all surfaces. The present work demonstrates that a dipolar induced-charge screening cloud generically forms around dielectric colloids, along with an associated (quadrupolar) ICEO slip velocity. This results in non-zero hydrodynamic interactions between suspended colloids during electrophoresis, giving velocity corrections of order  $\Delta u \sim U_0 a^2 / r^2$ , where  $r$  is the distance between particles. These corrections may be smaller than typical electrophoretic velocities, but they can play important roles in the evolution of the suspension, especially since they persist even in AC fields, where ‘standard’ electrophoresis would

give zero average motion. One example is shown in figure 6, where a suspension of metal colloids undergoing AC electrophoresis contracts along the field axis to form a disk-like suspension which spreads perpendicular to the applied field. This phenomenon suggests a method for probing surface properties of colloids based on ICEO interactions. Finally, we note that the electrophoresis of metallic particles is dominated by ICEO flows, which can be used to separate particles by size and shape in the presence of broken symmetries.

In this article, we have concentrated upon on the ICEO flow in systems of high symmetry: circular cylinders and spheres in spatially uniform applied fields, for which simple exact solutions are possible. In a companion article, we will explore the implications of broken spatial symmetries – both via asymmetric conductors and gradients in the applied electric field – and will explore further potential applications for microfluidic devices and colloidal separation methods. For a brief summary of our results, the reader is referred to Bazant & Squires (2003).

In conclusion, induced-charge electro-osmosis is a remarkably general and basic phenomenon, capable of producing large fluid ‘slip’ velocities around polarizable surfaces, under AC or DC fields. Many variants exist on the basic ICEO situations presented in this article; for example, one can apply spatially inhomogeneous electric fields, vary the geometry of the polarizable surface, apply fixed-potential (or actively-controlled potential) ICEO flows, and so on. ICEO opens a host of new possibilities for microfluidic and colloidal manipulation which we hope will soon be explored experimentally in real devices.

### Acknowledgments

The authors would like to thank École Supérieure de Physique et Chimie Industrielles (Laboratoire de Physico-chimie Théorique) for hospitality and partial support. This research was also supported in part by the U.S. Army through the Institute for Soldier Nanotechnologies, under Contract DAAD-19-02-0002 with the U.S. Army Research Office (MZB), and by the NSF Mathematical Sciences Postdoctoral Fellowship and Lee A. Dubridge Prize Postdoctoral Fellowship (TMS).

### Appendix A. Fixed-potential ICEO flow due to a cylinder grounded to a planar electrode

The total ICEO flow is given by the superposition of several flows: the standard fixed-charge ICEO flow around a conducting cylinder (2.10-2.11), with decay  $\sim r^{-1}$ , the fixed-potential ICEO flow (associated with 4.5), with decay  $\sim r^{-2}$ , the flow due to the force keeping the cylinder in place (4.7), which has a logarithmic decay, as well as the ‘image flows’ due to the wall. The leading-order approximation to the fixed-potential ICEO flow is then given by the forced flow and its images. The two-dimensional flow field due to a point force directed perpendicular to the wall was found by Liron & Blake(1981) to be

$$u_i = \frac{F_E}{4\pi\eta} \cdot [\mathbf{S}(\mathbf{R}) - \mathbf{S}(\mathbf{R}_0) + 2h^2 \mathbf{G}^D(\mathbf{R}_0) - 2h \mathbf{G}^{SD}(\mathbf{R}_0)], \quad (\text{A } 1)$$

where, following Pozrikidis(1992),  $\mathbf{R} = \mathbf{r} - \mathbf{r}_0$  is the vector connecting the observation point  $\mathbf{r}$  with the singularity location  $\mathbf{r}_0$  and  $\mathbf{R}_0 = \mathbf{r} - \mathbf{r}_0 + 2h\hat{\mathbf{z}}$  is the vector connecting the observation point with the image point  $\mathbf{r}_0 - 2h\hat{\mathbf{z}}$ . Here  $S_{ij}$  is the two-dimensional Stokeslet,

$$S_{ij} = -\log r \delta_{ij} + \frac{r_i r_j}{r^2}, \quad (\text{A } 2)$$

$G^D$  is the source dipole,

$$G_{ij}^D = - \left( \frac{\delta_{ij}}{r^2} - \frac{r_i r_j}{r^4} \right), \quad (\text{A } 3)$$

and  $G^{SD}$  is the Stokeslet doublet,

$$G_{ij}^{SD} = - \frac{\partial S_{iz}}{\partial z}. \quad (\text{A } 4)$$

## Appendix B. ICEO around a conducting cylinder with a dielectric coating

We consider the induced-charge electro-osmotic flow around a metal cylinder (region I,  $r < a$ ) which is coated by a thin layer (region II,  $a < r < b$ ) of dielectric  $\epsilon_2$ , immersed in an ionic solution (region III,  $r > b$ ) of dielectric constant  $\epsilon_w$ . An electric field  $E_0 \hat{z}$  is applied.

To calculate the ICEO slip velocity around a coated conducting cylinder, we first calculate the fields set up around a thin, dipolar charge double layer with time-dependent zeta potential  $\zeta_0(t) \cos \theta$ . A dipolar field is set up outside the charge cloud, and a constant field is set up inside. The coated cylinder is immersed in a constant field (charge cloud plus externally-applied), and a dipolar field is set up in response. The combination of these two dipolar fields (cylinder plus charge cloud) then give the normal electric field. As before, an ordinary differential equation is derived for the evolution of the zeta potential.

### B.1. Field induced by dipolar charge cloud

We assume the charge cloud is thin, so that  $\kappa b \gg 1$ , so that the charge cloud ‘looks’ locally planar, giving a charge cloud density

$$\rho = -\epsilon_w \kappa^2 \zeta_0 e^{-\kappa(r-b)} \cos \theta. \quad (\text{B } 1)$$

The potential due to the charges in the double layer can be found using the two-dimensional Green’s function,

$$\phi_{DL}(r_0, \theta_0) = - \int_b^\infty \int_0^{2\pi} \frac{\rho(r, \theta)}{4\pi\epsilon_w} \ln\{r^2 + r_0^2 - 2rr_0 \cos(\theta - \theta_0)\} r dr d\theta. \quad (\text{B } 2)$$

Because the double layer is thin, and because we are interested in the fields outside of the double layer, we expand the kernel, giving

$$-\ln\{r^2 + r_0^2 - 2rr_0 \cos(\theta - \theta_0)\} \sim 2\frac{r_0}{r} \cos(\theta - \theta_0) \quad (\text{B } 3)$$

inside the charge cloud ( $r < b$ ). An analogous expansion holds outside of the charge cloud, with  $r_0/r$  in place of  $r/r_0$ . The expansion term shown is the only one that survives the angular integration, giving a dipole field

$$\phi_{DL}^> = -\frac{\kappa \zeta_0}{2} \left( 1 + \frac{2}{\kappa b} \right) \frac{b^2 z_0}{r_0^2}. \quad (\text{B } 4)$$

outside the double layer, and

$$\phi_{DL}^< = -\frac{\kappa \zeta_0}{2} z_0 \quad (\text{B } 5)$$

inside the double layer.

The total field inside of the screening cloud,  $C_0$ , is given by

$$C_0 = \left( E_0 + \frac{\kappa \zeta_0}{2} \right). \quad (\text{B } 6)$$

### B.2. Field induced by coated conducting cylinder

We consider a coated, conducting cylinder immersed in a constant field  $C_0\hat{\mathbf{z}}$ . The potential in the dielectric layer ( $\phi_2$ ) and outside the cylinder ( $\phi_3$ ) are given by

$$\phi_2 = A_0 \left( r - \frac{a^2}{r} \right) \cos \theta \quad (\text{B } 7)$$

$$\phi_3 = \left( -C_0 r + D_0 \frac{b^2}{r} \right) \cos \theta \quad (\text{B } 8)$$

which satisfies the conducting boundary condition  $\phi_2(a) = 0$ . By enforcing the dielectric boundary conditions at the interface,

$$\epsilon_2 \frac{\partial \phi_2}{\partial r} \Big|_{r=b} = \epsilon_w \frac{\partial \phi_3}{\partial r} \Big|_{r=b} \quad (\text{B } 9)$$

$$\frac{\partial \phi_2}{\partial \theta} \Big|_{r=b} = \frac{\partial \phi_3}{\partial \theta} \Big|_{r=b}, \quad (\text{B } 10)$$

the constants are determined to be

$$A_0 = \frac{b^2}{b^2 - a^2} (D_0 - C_0) \quad (\text{B } 11)$$

$$D_0 = \Gamma_c C_0, \quad (\text{B } 12)$$

where

$$\Gamma_c = \frac{b^2 + a^2 - \epsilon_w/\epsilon_2(b^2 - a^2)}{b^2 + a^2 + \epsilon_w/\epsilon_2(b^2 - a^2)}. \quad (\text{B } 13)$$

### B.3. Total induced dipole

The total electrostatic potential outside the charge cloud consists of the applied field, the dipole induced by the charge cloud (B 4), and the dipole induced by the cylinder (B 8) immersed in the constant field (B 6), and is

$$\phi(t) = -E_0 r_0 \cos \theta + \left( \Gamma_c E_0 - \frac{\kappa \zeta_0}{2} \left[ 1 - \Gamma_c + \frac{2}{\kappa b} \right] \right) \frac{b^2 \cos \theta}{r_0}. \quad (\text{B } 14)$$

The perpendicular field just outside the double layer is given by

$$E_{\perp}(b) = E_0 \cos \theta + \left( \Gamma_c E_0 - \frac{\kappa \zeta_0}{2} \left[ 1 - \Gamma_c + \frac{2}{\kappa b} \right] \right) \cos \theta, \quad (\text{B } 15)$$

Equation 2.4 relates the evolution of  $\zeta_0$  to the normal field  $E_{\perp}$ , giving

$$\frac{d\zeta_0}{dt} = -\frac{(\zeta_0 - \zeta_s)}{\tau_c}, \quad (\text{B } 16)$$

where  $\zeta_s$  represents the steady-state induced-charge zeta potential,

$$\zeta_s = \frac{2E_0 b (1 + \Gamma_c)}{2 + \kappa b (1 - \Gamma_c)}, \quad (\text{B } 17)$$

and  $\tau_c$  is the time scale on which the charge cloud forms around the coated cylinder,

$$\tau_c = \frac{\epsilon_w \kappa}{\sigma} \left( 1 + \frac{\kappa b}{2} (1 - \Gamma_c) \right)^{-1} \equiv \frac{\lambda_D b}{D} \left( 1 + \frac{\kappa b}{2} (1 - \Gamma_c) \right)^{-1}. \quad (\text{B } 18)$$

- AJDARI, A. 1996 Generation of transverse fluid currents and forces by an electric field: Electroosmosis on charge-modulated and undulated surfaces. *Phys. Rev. E* **53**, 4996.
- AJDARI, A. 2000 Pumping liquids using asymmetric electrode arrays. *Phys. Rev. E* **61**, R45–R48.
- AJDARI, A., BAZANT, M. Z., AND THORNTON, K. 2003 Intermediate time scale in the relaxation of a dilute electrochemical cell, in preparation.
- BAZANT, M. Z. & SQUIRES, T. M. 2003 Induced-charge electrokinetic phenomena, in preparation.
- BEN, Y. & CHANG, H. C. 2002 Nonlinear Smoluchowski slip velocity and micro-vortex generation. *J. Fluid Mech.* **461**, 229–238.
- BONNEFONT, A., ARGOUL, F. & BAZANT, M. Z. 2001 Analysis of diffuse-layer effects on time-dependent interfacial kinetics. *J. Electroanal. Chem.* **500**, 52.
- BROWN, A. B. D., SMITH, C. G. & RENNIE, A. R. 2000 Pumping of water with AC electric fields applied to asymmetric pairs of microelectrodes. *Phys. Rev. E* **63**, 016305–8.
- DUKHIN, S. S. 1991 Electrokinetic phenomena of the 2nd kind and their applications. *Adv. Colloid Int. Sci.* **35**, 173–196.
- JEFFREY, D. J. & ONISHI, Y. 1981 The slow motion of a cylinder next to a plane wall. *Q. J. Mech. Appl. Math.* **34**, 129–137.
- LEVICH, V. G. 1962 *Physicochemical Hydrodynamics*. Englewood Cliffs, N.J.: Prentice-Hall.
- LIRON, N. & BLAKE, J. R. 1981 Existence of viscous eddies near boundaries. *J. Fluid Mech.* **107**, 109–129.
- MORRISON, F. A. 1970 Electrophoresis of a particle of arbitrary shape. *J. Colloid Interface Sci.* **34**, 210–214.
- NADAL, F., ARGOUL, F., HANUSSE, P., POULIGNY, B. & AJDARI, A. 2002 Electrically induced interactions between colloidal particles in the vicinity of a conducting plane. *Phys. Rev. E* **64**, 061409.
- O'BRIEN, R. W. & WHITE, L. R. 1978 Electrophoretic mobility of a spherical colloidal particle. *J. Chem. Soc. Faraday II* **74**, 1607–1626.
- POZRIKIDIS, C. 1992 *Boundary integral and singularity methods for linearized viscous flow*. Cambridge: Cambridge University Press.
- RAMOS, A., MORGAN, H., GREEN, N. G. & CASTELLANOS, A. 1999 AC electric-field-induced fluid flow in microelectrodes. *J. Colloid Int. Sci.* **32**, 420–422.
- RUSSEL, W. B., SAVILLE, D. A. & SCHOWALTER, W. R. 1989 *Colloidal Dispersions*. Cambridge: Cambridge University Press.
- STONE, H. A. & SAMUEL, A. D. T. 1996 Propulsion of microorganisms by surface distortions. *Phys. Rev. Lett.* **77**, 4102–4104.
- TAYLOR, G. I. 1966 The circulation produced in a drop by an electric field. *Proc. Roy. Soc. A* **291**, 159–166.
- THAMIDA, S. K. & CHANG, H.-C. 2002 Nonlinear electrokinetic ejection and entrainment due to polarization at nearly insulated wedges. *Phys. Fluids* **14**, 4315–4328.
- TRAU, M., SAVILLE, D. A. & AKSAY, I. A. 1997 Assembly of colloidal crystals at electrode interfaces. *Langmuir* **13**, 6375–6381.
- YEH, S. R., SEUL, M. & SHRAIMAN, B. I. 1997 Assembly of ordered colloidal aggregates by electric-field-induced fluid flow. *Nature* **386**, 57–59.